Delft University of Technology

Self-catalysed frontal polymerisation enables fast and low-energy processing of fibre reinforced polymer composites

Staal, Jeroen; Caglar, Baris; Michaud, Véronique

Important note
To cite this publication, please use the final published version (if applicable).
Please check the document version above.

Contents lists available at ScienceDirect

Composites Science and Technology

Self-catalysed frontal polymerisation enables fast and low-energy processing of fibre reinforced polymer composites

Jeroen Staal [a], Baris Caglar [b], Véronique Michaud [a],[*]

[a] *Laboratory for Processing of Advanced Composites (LPAC), Institute of Materials, Ecole Polytechnique Fédérale de Lausanne (EPFL), Lausanne, Switzerland*
[b] *Aerospace Structures and Materials Department, Faculty of Aerospace Engineering, Delft University of Technology, Delft, the Netherlands*

ARTICLE INFO

ABSTRACT

Frontal polymerisation has the potential to bring unprecedented reductions in energy demand and process time to produce fibre reinforced polymer composites. Production of epoxy-based fibre reinforced polymer parts with high fibre volume content, commonly encountered in industry, is however hindered by the heat sink created by the fibres and the mould, overcoming the heat output of the chemical reaction, thus preventing front propagation. We propose a novel self-catalysed frontal polymerisation manufacturing method based on the integration of thin resin channels in thermal contact with the composite stack as a strategy for low-energy production of high fibre volume fraction polymer composites without the need for a continuous energy input. Frontal polymerisation inside the resin channel proceeds faster and preheats the fabric stack, thus catalysing the process. Parts with up to 60% fibre content are successfully produced independently of the sample thickness. Fillers added within the resin channels provide means to tailor the frontal polymerisation process kinetics. The parts have a significantly higher glass transition temperature than those produced in a conventional oven, and comparable mechanical properties while energy consumption is reduced by over 99.5%.

1. Introduction

Fibre reinforced polymer composites have become widely applied in structural applications in industries such as aerospace [1,2], transport [3] and energy [4]. Production of FRP parts with thermoset matrices typically requires thermal cure cycles in an oven, heated mould or autoclave, which can take several hours up to days [5,6]. This step makes FRP processing generally slow with a large environmental footprint while imposing excessive tooling costs for large, e.g. airplane or wind turbine, parts [5,6]. Driven by the search for more efficient and sustainable FRP production methods, a variety of novel curing methods have been proposed that could each reduce the processing time and/or the required energy input [6]. Frontal polymerisation (FP) emerges as a particularly promising approach as it has the potential to cure FRP parts in minutes with little external energy input [7,8]. Governed by the released polymerisation enthalpy, FP systems can form an autocatalytically-induced front between hot (>200 °C) formed polymer and cold monomer resin, after the local application of an initial external stimulus (e.g. heat or UV-irradiation). The front propagates autonomously through the impregnated fibrous preform until the composite is fully cured, as long as a threshold activation energy for enabling of the autocatalytic mechanism is exceeded [9].

Current FP systems can be subdivided into two classes: those that undergo frontal ring opening metathesis polymerisation (FROMP) and systems capable of radical induced cationic frontal polymerisation (RICFP). FROMP systems, e.g. based on poly(dicyclopentadiene), have shown excellent front characteristics due to the highly reactive nature of the underlying free-radical chemistry [10–14] and a potential of recycling [15,16], but are limited by their relatively short pot life of only a few hours [17]. RICFP systems on the other hand are known for their remarkable stability, e.g. over a month when stored at 50 °C in a dark environment [18], and are capable of producing epoxide polymer [19–21], which is already widely applied in the FRP industry, but their high exothermicity, as compared to acrylate systems, and relatively low reactivity makes them less favourable for FP [14].

Successful FP of FRPs requires precise control of the local heat balance between the resin reaction enthalpy, thermal diffusion and heat losses to the environment and fibrous reinforcements. With the latter term becoming increasingly significant with increasing fibre volume content (V_f), a system-dependent maximum defines the V_f where the available activation energy falls below the threshold, resulting in premature quenching of the front [7,9]. Laboratory scale examples are still

well below the industrial standard in terms of fibre content, i.e. RICFP has been demonstrated for carbon V_fs of up to 35% [22], 40% [23] while FROMP is reportedly possible up to 50% [10,24]. We have recently demonstrated [25] that the maximum V_f of a RICFP system could be extended by adequate tuning of the resin composition and thermal management by the use of a highly insulating process configuration, defining a system limit of 45.8% for carbon fibre reinforcements that is already much closer to applications than in previous studies. Industrialisation of FP-assisted FRP processing thus requires overcoming these limitations. Strategies so far towards applications of FP comprise the intrinsic optimisation of the system by maximization of the heat release rate, via the development of highly reactive initiators [23,26–29] and resin compositions [18,19,22,25,30], or the minimization of heat losses to the environment [25,31]. Alternative strategies such as pre-heating [10,24] or oven-heating [32] of the system or relying on the application [15] or integration [31] of resistive heaters have shown to be effective but these add to the energy input of the process and reduce the advantage of FP being a versatile, low-energy FRP processing method.

In parallel, resin channels are frequently introduced in composite manufacturing to improve the impregnation kinetics of fibrous preforms in liquid composite moulding configurations. While these high-permeability channels can be created within the fabric stacks [33], flow kinetics are often enhanced by spacers [34] and by grooved or porous layers [35] that are placed on top of the fabric stacks. Optimised placement of these structures [36–38] strongly reduces the impregnation time [35] while they can be removed after the curing process and hence do not affect the resulting FRP properties. With inspiration from the industrial practice to optimise the impregnation processes via sacrificial layers, we propose here a novel self-catalysed processing approach whereby a parallel FP resin channel enhances and tunes the local heat balance of an FRP system. Using a typical epoxide system capable of RICFP, we demonstrate that with this approach, FRPs with a fibre content in the 60% range, i.e. 15-25% higher than reported in previous studies, can be produced without the need of any (dis)continuous external energy source, bridging the gap towards sustainable and

efficient processing of industrial FRPs. This work outlines the potential of self-catalysed frontal polymerisation by providing an overview of process characteristics and the role of several process parameters (e.g. composite thickness and filler type) followed by an assessment of process control through variation of the resin channel composition. Finally, an analysis of the resulting FRP properties in comparison to those produced by conventional oven-curing is provided.

2. Results

2.1. Process configuration

With the resin composition used in the present work, FRPs were first successfully produced in a highly insulating conventional mould configuration, without a sacrificial resin channel, for parts with a carbon fibre V_f up to 41.8%. This fibre content is slightly lower than the 45.8% reported [25] for a vacuum-assisted hand layup configuration; this is attributed to the higher heat uptake of the foam top mould as compared to a vacuum bag/air interface. Fig. 1a compares the highest fibre contents reported in the literature and shows that this V_f approaches the currently reported maxima for RICFP systems while it is significantly lower than the maxima reported for FROMP systems, both of which are nevertheless below the industrially relevant range for structural applications (V_f >55%). To overcome this limit, we propose a novel self-catalysed frontal polymerisation process where a sacrificial resin channel is placed on top of the impregnated fabric stack and separated by a rigid membrane. This process configuration, schematically shown in Fig. 1b, has the potential to enhance the front characteristics of a given resin-fibre system without the need for any (dis)continuous energy input.

As for most conventional FRP manufacturing processes, the self-catalysed FP processing method comprises an impregnation and a curing phase. Impregnation of the fabric stack and sacrificial resin channel is carried out simultaneously. The large permeability difference between these sections requires the integration of a resin barrier in the
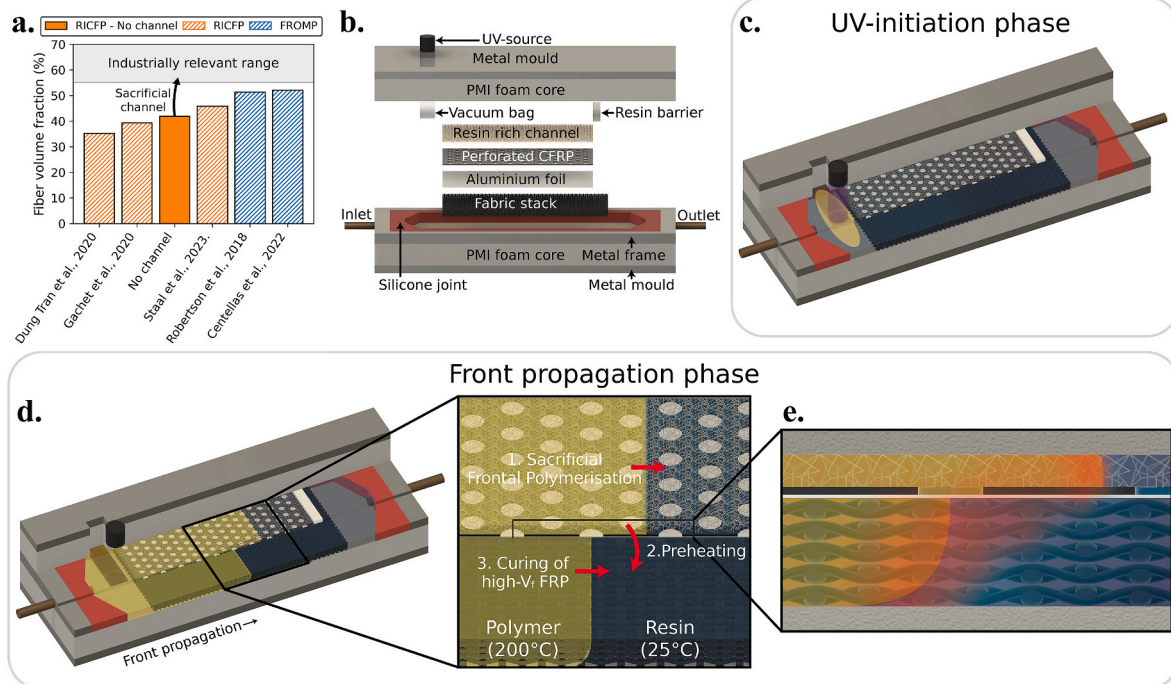
Fig. 1. Overview of the self-catalysed FP process. **(a)** Comparative overview of maximum fibre volume contents reported for FP processing of FRPs without continuous external energy input. **(b)** Transverse exploded view of the self-catalysed FP mould configuration. **(c)** Sliced view illustrating front initiation by UV-irradiation. **(d)** Sliced view illustrating the front propagation phase by 1. FP of the resin channel, 2. Heat transfer to the fabric stack and 3. FP of the high V_f fabric stack. **(e)** Cross-section near the front region with the expected heat flow indicated in red.

channel to avoid the resin race-tracking through this section, leaving the fabric stack unsaturated.

Once the fibres are completely saturated, a polymerisation front is initiated in the resin-rich section of the mould, i.e. as shown in Fig. 1c, by localised UV-irradiation. The front propagates autocatalytically until the fabric/channel section is reached. In the resin channel, since there are no fillers, hence less energy loss, the front continues to propagate. FP in the fabric stack on the other hand is delayed, as illustrated in Fig. 1d, since the heat loss to the fibres is such that the activation energy threshold can initially not be exceeded. As heat propagates from the resin channel to the fibre-rich cavity, resulting from the frontal polymerisation of the resin channel, the temperature of the fabric stack rapidly increases, i.e. to 50–100 °C within several tens of seconds. A secondary front thus propagates through the fabric stack once the temperature in the fabric stack is sufficiently high to sustain FP, allowing for successful frontal polymerisation of FRPs with significantly increased V_{fs}. This configuration moreover brings the advantage that an external energy input is only required during the initiation stage, i.e. to form a polymerisation front in the resin rich section. The heat transfer between

the channel and the fabric stack needs to be tuned to achieve an optimal processing strategy. This was largely achieved via the separator, which ideally possesses a high thermal conductivity in through-thickness direction, i.e. to maximize the heat transfer from the resin channel to the fabric stack, and a lower conductivity in the in-plane direction to avoid excessive spreading of the reaction front. Moreover, the separator must be sufficiently stiff to avoid deformation by the compacted fabric stacks and to maintain a constant channel geometry, resulting in maximum sample flatness. The combination of a perforated carbon FRP plate and an aluminium foil layer was chosen as the preferred combination to fulfil these requirements over e.g. metallic or Teflon separators. The optimised experimental configuration is illustrated in more detail in Appendix A.

2.2. Temperature profiles during self-catalysed FP processing

The geometry of the resin channel was designed to ensure sufficient preheating of the fabric stack. Fig. 2a displays recorded temperature profiles for the cases of thermally conductive carbon and insulating glass
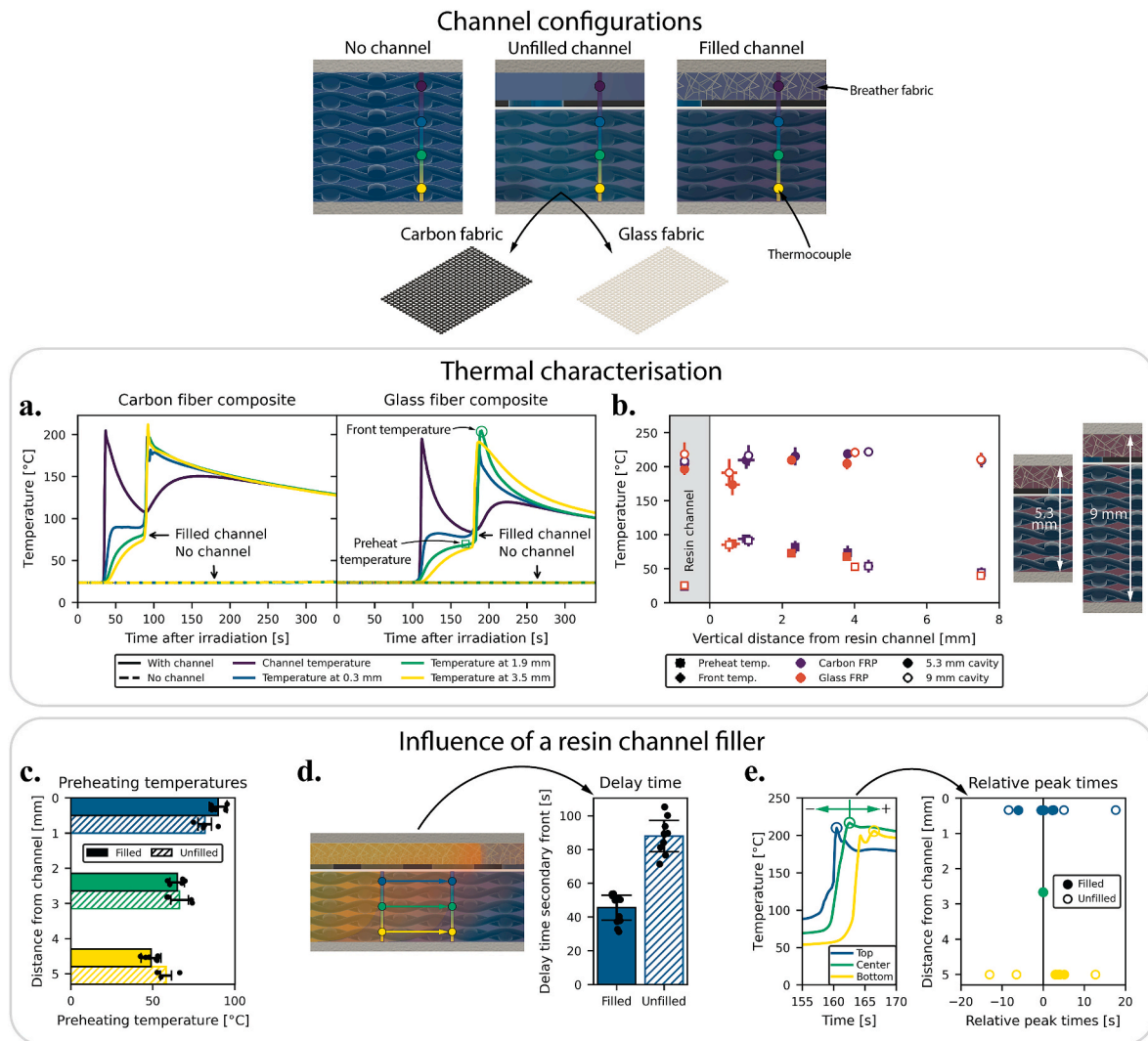

Fig. 2. Comparison of thermal and front characteristics in different mould configurations. Distances are defined relative to the resin channel/separator and all thermocouples were placed at two-thirds of the fabric length, i.e. ~70 mm from the point of initiation, at various depths through the composite thickness. **(a)** Exemplary temperature profiles recorded for carbon and glass FRPs with overall composite thicknesses of 3.6 mm during RICFP processing with and without the presence of a sacrificial resin channel. **(b)** Average recorded preheating and front temperatures in carbon and glass FRPs at different positions for 5.3 mm and 9 mm thick mould cavities. **(c)** Preheating temperatures at different vertical positions in filled and unfilled mould configurations. **(d)** Mean delay times between fronts in filled and unfilled resin channels and the secondary fronts recorded at two-thirds of the fabric length. **(e)** Influence of resin channel fillers on the peak times recorded at different vertical positions in the fabric stack relative to the middle thermocouple positions.

fibre reinforcements at V$_f$s of ~50–55%. In this configuration and in the absence of a resin channel, the available RICFP resin could not provide the energy to overcome the heat losses and hence no temperature increase corresponding to self-sustaining frontal polymerisation was observed. Recordings made in a self-catalysed FP configuration, with a resin channel of about 1.5 mm thick, on the other hand showed distinct thermal peaks that confirmed the occurrence of self-sustaining frontal polymerisation. The delayed front propagation in the FRP stack, illustrated in Fig. 1d, is observed in Fig. 2a when comparing the thermal peaks inside the resin channel, and inside the fabric at the same location over the mould length. The conductive aluminium separator layer ensured for rapid heat transfer upon FP of the resin channel, resulting in a fast temperature increase at the top of the fabric stack, reaching a temperature of ~85 °C within 10–15 s while the temperature increase was more gradual at lower thermocouple positions. The slow cooling after the occurrence of the thermal peaks, corresponding to FP, is attributed to the insulating mould configuration, and we have previously reported [25] that this is highly beneficial for the resulting curing degree.

The experimental configuration was designed to be compatible with the two most common reinforcements in the composites industry, namely thermally conductive carbon and insulating glass reinforcements. The resulting front behaviour in Fig. 2a only showed minor differences between carbon and glass FRPs, which are inherent to their different intrinsic thermal properties. The lower thermal conductivity of glass fabrics delayed the heat transfer and thereby the preheating rates throughout the fabric stack. This was further evidenced by the reduced velocity of the secondary front, which is commonly observed in the presence of low thermal conductivity fillers [39–41], resulting in similar preheating temperatures before the onset of FP. The self-catalysed FP process is thus suggested to have self-adaptive capabilities based on its constituents, as long as sufficient energy is provided to overcome the activation energy threshold.

An evaluation of the influence of the fabric stack thickness, while maintaining the same resin channel geometry, was carried out to further assess the potential of producing thicker FRPs and hence to widen the potential range of applications of the self-catalysed FP processing method. Preheating and front temperatures were recorded by four thermocouples that were integrated at different vertical positions in the resin channel and fabric stack. Front temperature corresponds to the maximum recorded temperature, i.e. at the arrival of the polymerisation front, while the preheating temperature is defined as the temperature right before the onset of FP. Fig. 2b shows the preheating and front temperatures for both considered fabric types in a 5.3 mm cavity and in a 9 mm cavity, while the experimental data is reported in more detail in Appendix B. With a constant resin channel thickness of 1.5 mm imposed by spacers, and the thickness of the separator (~0.2 mm), these cavity heights resulted in FRP thicknesses of about 3.6 and 7.3 mm for the respective 5.3- and 9-mm cavities. The preheating temperature close to the resin channel was comparable for all configurations, i.e. a range of 85–95 °C, as it mainly depends on the rapid heat transfer from the polymerising resin channel. The front temperature in this section was however lower than that recorded deeper into the fabric stack. This was in particular observed for glass FRPs where the front temperature was reduced by ~25–35 °C. Supported by differential scanning calorimetry measurements reported in Appendix C, this was attributed to minor precuring of the resin during the delay period between the FP of the resin channel and the arrival of the secondary front, despite preheating temperatures remaining below the estimated onset of the autocatalytic reaction mechanism (also Appendix C). This pre-curing is believed to have reduced the available epoxide groups and thereby the polymerisation enthalpy that can be released upon FP, resulting in a front temperature that is below the expected range for a pristine system [25], i.e. >200 °C. The extent of pre-curing was sufficiently low to allow for successful FP and the lengthy cooling phase is believed to overcome potential minor decreases in the curing degree induced by the lower

front temperature.

The recorded preheating temperature slightly decreased with the distance from the resin channel. A comparison in Fig. 2b shows that the preheating temperature in a 9 mm cavity mould was lower, i.e. 52.9 ± 4.4 °C at 4 mm distance in a glass FRP system, compared to the temperature of 72.8 ± 4.0 °C recorded at a similar position in a 5.3 mm mould cavity. This is attributed to the increased heat sink and diffusion effect due to presence of more fibres and more resin at the increased cavity height. Since roughly the same amount of thermal energy is provided by the resin channel, the average preheating temperature would thus be expected to be lower in a 9 mm cavity. The resulting front temperature was however comparable for thermocouple positions that were over ~1 mm from the resin channel and in line with the expected front temperatures of this RICFP system [25]. This suggests that the preheating temperature induced by the designed sacrificial resin channel geometry provides sufficient energy to, combined with the activation energy provided by the propagating front, induce a shift in the maximum allowed V$_f$ while maintaining comparable front characteristics. Further variation of the resin channel, e.g. its geometry, may enable fine-tuning of the local heat balance and thereby the FP behaviour in high-V$_f$ composites.

2.3. Control of the front morphology by channel fillers

The presence of fillers in the resin channel was found to significantly influence the front characteristics of the secondary front. To illustrate this dependence and its potential to control the self-catalysed FP process, carbon FRPs of ~55% V$_f$ were produced using resin channels either filled with a low-V$_f$ thermally insulating breather fabric, i.e. a non-woven polyester mat frequently used for guiding air flow in FRP production, or unfilled resin channels. Filling the resin channel with a strip of breather fabric corresponded to a V$_f$ of ~7.5% which was believed to be, in line with prior reports [39–41] on the use of insulating fillers, sufficient to reduce the front velocity inside the resin channel. Propagation of the channel and secondary fronts typically resulted in smooth temperature profiles, e.g. similar as shown for carbon FRP in Fig. 2a, when a strip of breather fabric was placed in the resin channel. In the presence of the filler material, preheating temperatures in a 7.3 mm cavity shown in Fig. 2c ranged from 89.9 ± 4.2 °C close to the resin channel to 64.9 ± 4.4 °C and 48.9 ± 3.9 °C in the middle and bottom of the fabric stack, respectively. The delay between the passing of both fronts was on average 46.4 ± 5.8 s, as displayed in Fig. 2d.

The use of an unfilled resin channel was expected to increase the available energy for heat transfer and hence increase the preheating temperature and front characteristics of the secondary front. The delay time in this configuration (Fig. 2d) was with 94.7 ± 6.6 s nearly double that of when a breather strip was placed in the resin channel; this was attributed to the increased difference in front velocities between the channel and secondary fronts. Fig. 2c however shows that this extended delay only slightly increased the preheating temperature recorded by the bottom and middle thermocouples to respectively 58.0 ± 6.0 °C and 66.3 ± 7.4 °C while the preheating temperature closest to the channel was even lower, i.e. 81.7 ± 5.4 °C as compared to 89.9 ± 4.2 °C when a filled resin channel was used. This is attributed to the extensive delay that resulted in cooling down of the preheated resin as also shown Appendix D.

Experimental configurations using an unfilled resin channel moreover showed significant inconsistencies in the peak times and temperature profiles (see Appendix D). The peak times, i.e. corresponding to the arrival of the front at the thermocouple position, were used to obtain a further indication of the front morphology. Fig. 2e presents the relative peak time as compared to the peak time of the middle thermocouple position and shows that there was no apparent trend in the peak times for a system with an unfilled resin channel, suggesting that no consistent front morphology was present. The more uniform preheat temperatures in combination with increased precuring due to the larger delay times,

may result in the formation of a discontinuous front that propagates when enough activation energy is present locally. Configurations where the resin channel was filled with breather fabric on the other hand showed good correlation on the relative peak times between samples in Fig. 2e. The short delay between the top and middle thermocouple positions combined with the slight lag of the lower thermocouple suggests a hypothetical front morphology as illustrated in Fig. 1e. Although further investigation is required to elucidate the exact role of resin channel fillers, the observations presented in this section highlight the potential of controlling the self-catalysed FP process by the addition of fillers in the resin channel. An optimum solution is expected to balance the heat flow, inducing the formation of a consistent front morphology while also ensuring a sufficiently high compressive stiffness to resist against deformation by the compressed high-V_f fabric stacks.

2.4. Comparison between self-catalysed and oven-cured FRPs

The energy demand, glass transition temperature, and mechanical properties, i.e. ILSS and Young's modulus, of FRPs produced by the proposed self-catalysed FP methodology were compared to oven-cured FRPs that were produced with either the same RICFP resin or Sicomin and Araldite commercial resins. A comparative overview of the resulting properties can be found in Fig. 3a and in Appendix E. The self-catalysed FP processing method required only a fraction of the energy demand for front initiation by UV-irradiation, as compared to the energy consumption recorded during the lengthy oven-curing procedures prescribed to produce FRP parts with commercial Sicomin and Araldite resins, requiring respective external energy inputs of 1.994 ± 0.000 and 7.142 ± 0.047 kWh. Replacement of these resins by a RICFP resin allowed for the formation of a front after an initial preheating period, as observed from the temperature profiles shown in Appendix F, strongly

reducing the required curing time and hence the energy demand, in line with Ref. [42], to 0.434 ± 0.026 kWh. Integration of a sacrificial resin channel allowed for the production of FRPs with an average V_f of $59.1 \pm 2.0\%$, where the V_f variation originated from the variability in the compression characteristics of the preform and of the sacrificial layer, and V_fs of individual FRPs reaching up to 62.2%. A further reduction of the required energy input, solely resulting from UV-irradiation, of 99.5% was moreover observed. This reduction translates to a strongly increased number of parts that can be produced per unit energy which is, as shown in Fig. 3a, several orders of magnitude higher for self-catalysed FP as compared to its oven-cured alternatives. Moreover, since energy input is only required to initiate the FP process, and is hence independent of the part size, this difference is expected to increase when larger samples are produced.

The glass transition temperature (T_g) of FRPs produced by the self-catalysed FP process were significantly higher than that of oven-cured RICFP FRPs as shown in Fig. 3a. The T_g ratio of oven-cured RICFP FRPs moreover indicates that its T_g after the initial curing cycle was only $89.2 \pm 5.4\%$ of its maximum attainable T_g, i.e. the T_g after being subjected to a second thermal cycle in Dynamic Mechanical Analysis (DMA) measurements. This suggests that the maximum attainable monomer conversion was not achieved during the oven-curing cycle, which is likely a result of the fast temperature decrease in the presence of a metal mould [25], as demonstrated in Appendix F, and hence the absence of an intrinsic post-treatment upon passing of the front. The insulating nature of the foam-core mould allowed self-catalysed FP-produced FRPs to nearly reach their maximum attainable conversion without a postcuring treatment, i.e. only a minor increase in T_g was observed upon a second DMA cycle, which was also the case for oven-cured FRPs produced with commercial resin formulations. This is supported by the tan(δ) curves, corresponding to the phase angle between storage and loss moduli,
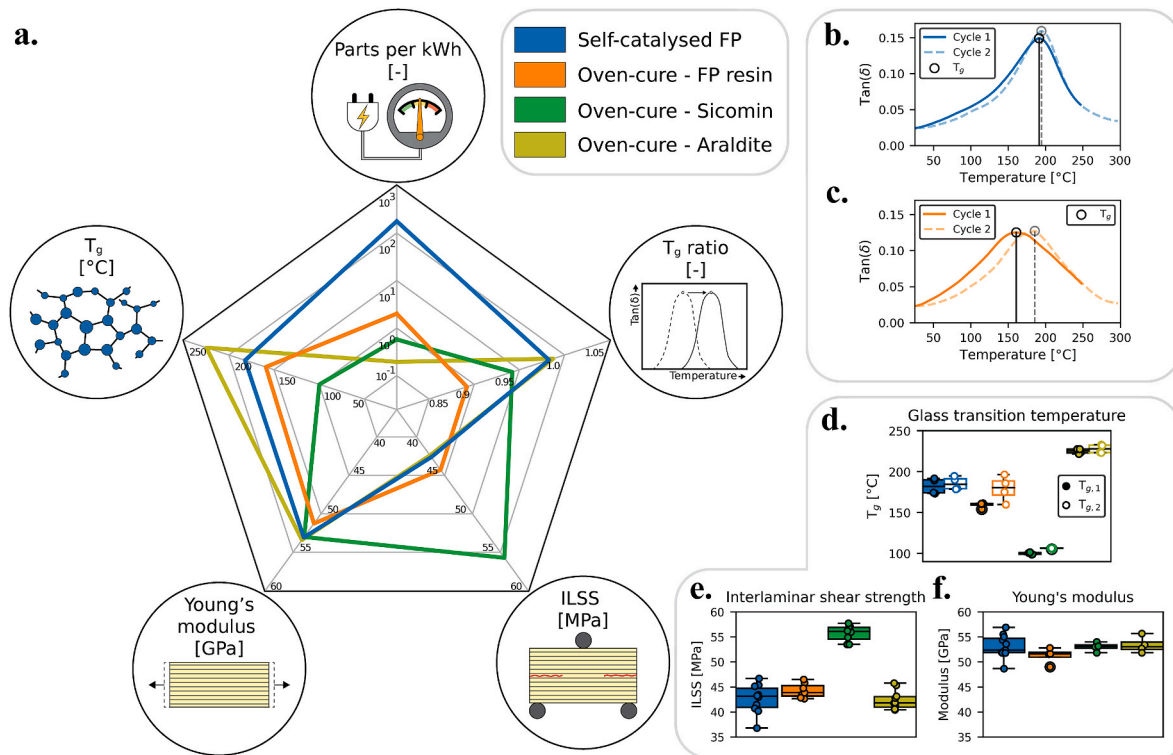

Fig. 3. Properties of FRPs produced by self-catalysed FP processing and conventional oven-curing. **(a)** Comparative overview of all recorded properties. The number of parts that could be produced per kWh was derived from the characterised energy demand. T_g ratio defines the ratio between the maximum attainable T_g, i.e. after a second DMA cycle, and the T_g of pristine FRP samples. **(b)** Exemplary tan(δ) curves of a carbon FRP produced by self-catalysed FP indicating the minor shift in T_g between heating cycles. **(c)** Similar exemplary tan(δ) curves of a carbon FRP produced by oven-curing using the RICFP resin, indicating a significant shift in T_g between heating cycles. **(d)** Boxplot indicating the statistical variability of T_g recordings. **(e)** Distribution of interlaminar shear strength recordings. **(f)** Variability of Young's modulus in recorded FRP samples.

recorded during DMA measurements of self-catalysed and oven-cured RICFP carbon FRPs in Fig. 3b and c, respectively. The tan(δ) curve of the self-catalysed RICFP FRP moreover showed a sharper peak, which suggests a more homogeneous cross-linking density to be present.

Self-catalysed RICFP FRPs however showed increased scatter in the T_g values compared to the reference samples as can be observed from Fig. 3d. This is largely believed to result from the inherent variation in compaction and nesting of the fabric stack that ultimately induces small changes in the in the channel geometry. These variations in channel thickness, and hence available heat transfer to the fabric stack, could induce (localised) differences in preheating and front temperatures, resulting in different degrees of cross-linking within the FRP part. The deformations moreover introduced small thickness variations in the self-catalysed FP FRP samples, potentially inducing an experimental inaccuracy in the DMA recordings. Further optimisation of the resin channel geometry is expected to overcome these deviations, allowing to optimally benefit from the presence of a sacrificial resin channel in RICFP FRP processing.

Evaluation of the mechanical properties by assessment of the interlaminar shear strength (ILSS) and Young's moduli showed similar behaviour for self-catalysed and oven-cured RICFP FRPs, as well as the oven-cured Araldite FRPs. While showing increased scatter due to the geometrical deviations in the resin channel, illustrated in Fig. 3e and f, the resulting properties suggest that the newly proposed self-catalysed FP processing strategy does not compromise the mechanical behaviour of its resulting FRPs. Further improvement of these properties, i.e. increasing the ILSS to match that of oven-cured Sicomin FRPs, could likely be achieved by further optimisation of the monomer composition while maintaining control over the front characteristics via extensive process control.

3. Conclusion

Manufacturing of FRPs by means of FP has the potential to bring large reductions in processing time and energy cost to the composite industry. The high V_fs typically sought for in the FRP industry lead to a significant heat uptake by the reinforcement, impeding current efforts to develop FP processing of FRPs. Using a model resin capable of radical induced cationic frontal polymerisation, this work presents a novel self-catalysed FP manufacturing strategy that overcomes these limitations without requiring additional energy input. This method is based on the placement of a sacrificial resin channel in thermal contact with the FRP part, allowing for effective preheating of the high-V_f impregnated preforms, lowering the activation energy threshold and hence enabling FP at V_fs in the 60% range that would normally see fronts being quenched. The method was found compatible with both conductive and insulating fibre types at a wide range of FRP thicknesses while thermal analysis suggested the process to be self-adaptive based on the constituents and geometry. The presence of a filler material in the resin channel was found to be of large influence on the frontal polymerisation process, reducing the front velocity while also inducing a more consistent front morphology. A comparison with conventional oven-cured FRPs showed that the novel self-catalysed FP processing method results in comparable mechanical properties while requiring only a fraction of the total energy cost. Analysis of the glass transition temperatures moreover showed self-catalysed FP processing to be favourable over oven-curing of the FP resin. These combined findings confirm the promising potential of the developed self-catalysed FP methodology as a strategy for fast and energy-efficient manufacturing of FRPs. Future work comprises the optimisation of the process by increased control over the heat flow in combination with the adaptation of self-catalysed FP processing for implementation in other conventional FRP processing methods.

4. Experimental methods

4.1. Materials

3,4-epoxycyclohexylmethyl-3′,4′-epoxycyclohexane carboxylate resin (UViscure S105, Lambson, United Kingdom), p-(octyloxyphenyl) phenyl iodonium hexafluorostibate (ABCR, Germany), thermal initiator benzopinacol (Thermo Fischer scientific, Belgium), iso-propylthioxanthone (Genocure ITX, Rahn, Switzerland), poly-methacrylimide foam (110 kg/m³, Rohacell IG-F 110, Evonik, Germany), carbon 2 × 2 twill weave fabric (285 g/m², ends/picks 3.5/ 3.5 cm⁻¹, 6K fibres/yarn, Suter Kunststoffe, Switzerland), E-glass 2 × 2 twill weave fabric (390 g/m², ends/picks 6/6.7 cm⁻¹, Suter Kunststoffe, Switzerland), polyester breather fabric (150 g/m², gore-tex (Suter Kunststoffe, Switzerland), high-temperature vacuum bag (Diatex Polyimide HM, Diatex, France), Sicomin SR8100 resin and 8822 hardener (Sicomin, France), Araldite LY 8615US resin and Aradur 8615 hardener (Huntsman, Switzerland).

4.2. Resin preparation

Resin preparation commenced by drying of the 3,4-epoxycyclohexylmethyl-3′,4′-epoxycyclohexane carboxylate resin in a vacuum chamber for 24 h. Cationic photoinitiator p-(octyloxyphenyl)phenyl iodonium hexafluorostibate, free-radical thermal initiator benzopinacol, and photosensitizer isopropylthioxanthone were added at concentrations of 0.75, 2.13 and 0.05 phr, respectively, and mixed under high shear rate until dissolved. Resins were degassed under vacuum at room temperature for a minimum of 30 min prior to the start of the experiment.

4.3. Self-catalysed RICFP processing

FRPs were produced in a polymethacrylimide foam mould that was covered by a thin layer of Teflon to allow facile release of the polymerised sample. Mould cavities were defined by in-house produced frames with a silicon joint placed inside the cavity to avoid leakage of resin. Carbon 2 × 2 twill weave and E-glass 2 × 2 twill weave fabrics were used as composite reinforcement. Fabrics were manually cut in strips of 100 × 50 mm and subsequently stacked in the mould cavity. A gore-tex flap was placed over the last 20 mm of the fabric stack as a resin barrier while the remaining section of the fabric stack was covered with an aluminium foil layer upon which a 0.2 mm thick perforated carbon FRP separator was placed. 1.5 mm thick aluminium strips were placed at the edges of the carbon FRP separator to define a resin channel with a controlled height. This resin channel was filled with strips of polyester breather fabric or left empty. An illustration of the experimental configuration can be found in Appendix A. The fabric stack and resin channel were simultaneously impregnated under a constant flow rate of 30 mL/h using a Razel Scientific Instruments R-100e syringe pump. FP was initiated by high intensity (>850 mW/cm²) UV-irradiation (EXFO Omnicure S2000) through an opening in the mould half covered with a layer of high-temperature vacuum bag. Produced composites were left to cool for a minimum of 10–15 min after completion of the FP process while remaining enclosed in the mould cavity. Fibre volume fractions were determined via following relation:

$$V_f = \frac{nA}{h\rho} \tag{1}$$

where n is the number of fabric layers, A the areal weight, h is the average resulting FRP thickness and ρ the fibre density, taken as 1.8 and 2.6 g/cm³ for carbon and glass fibres, respectively.

4.4. Temperature profiles

Preheating and front temperatures in self-catalysed FP processing were measured for both carbon and glass fibre preforms, of about 50–53% V_f, in 5.3- and 9-mm mould cavities. Temperature profiles were recorded by four 0.1 mm K-type thermocouples that were connected to a National Instruments DAQ device coupled to an in-house written Lab-View program. The thermocouples were embedded at the bottom, centre and top of the fabric stack, as well as on top of the breather fabric filler inside the resin channel, at about 65–70 mm of the fabric length in front direction. Recordings were started simultaneously with the start of UV-irradiation and data was acquired at a frequency of 100 Hz. Peak temperatures were defined as the maximum recorded temperature while preheat temperatures were taken as the temperature 10 s before the appearance of the peak.

4.5. Resin channel fillers

The influence of fillers in the resin channel was assessed using FRPs composed of 18 layers of carbon twill weave fabric and a mould cavity height of 7.3 mm. Resin channels were either filled with a strip of breather fabric or left empty. In the latter case, $2 \times 2 \times 1.5$ mm alumina cubes were placed at the front and end of the resin channel to avoid bending of the separator. Two series of three thermocouples were placed at the top, centre and bottom of the fabric stack. The separation distance was measured optically from images taken during the placement of the thermocouples and equalled ~0.8 cm. Delay times were defined as the time between the initial increase of the top thermocouple, corresponding to the passing of the front in the resin channel, and the recorded peak temperature at that thermocouple position.

4.6. Mechanical assessment

A comparative assessment was made between self-catalysed FP FRPs and oven-cured FRPs. Self-catalysed FP FRPs were produced in a 7.3 mm mould cavity. 18 layers of carbon twill fabric, corresponding to a V_f of 55–60% depending on the sample thickness, were stacked and the energy consumption during UV-irradiation was recorded by a Voltcraft SEM6000 device placed in series with the UV-source. Oven-cured reference samples were produced with three different resin types, i.e. the previously described RICFP resin, Sicomin SR8100 and Sicomin 8822 hardener or Araldite LY 8615US and Aradur 8615 hardener. All reference samples were produced with 18 layers of carbon twill fabric in the absence of a resin channel, while the mould was composed of steel mould halves with a cavity height of 5.3 mm. Impregnation of the fabric stacks was carried out at a constant rate of 30 mL/h. Oven-cured RICFP samples were placed in an oven (Reinhart Binder FD-115, Germany) at 150 °C after impregnation was completed while recording the temperature at the centre of the fabric stack via an integrated thermocouple. The mould was removed after 25 min and left to cool at room temperature. Sicomin and Araldite samples were cured following their respective prescribed procedures, i.e. Sicomin samples were post-cured for 8 h at 80 °C after an initial 24 h at room temperature while Araldite samples were cured for 24, 2 and 3 h at respectively 40, 120 and 180 °C. The energy consumption of the oven-curing procedures was recorded by placement of the Voltcraft SEM6000 device in series with the oven.

Glass transition temperatures (T_gs) were characterised by Dynamic Mechanical Analysis (DMA, TA Instruments DMA Q800) in three-point bending mode with an oscillation strain and frequency set to 0.1% and 1 Hz, respectively. Samples were cut to strips of $55 \times 10 \times 5.3$ mm parallel to the front direction and a minimum of three measurements were made per sample type. Measurements consisted of two successive heating cycles from 15 to 250 °C and 15 to 300 °C at a rate of 3 °C/min. The T_g of each cycle was determined from the maximum of the tan(δ) curve, representing the phase angle between storage and loss moduli.

Interlaminar shear strength (ILSS) of composite samples was char-acterised following ASTM standard D2344 on a universal tensile machine (UTM) Series LFM-125 kN (Walter & Bai, Switzerland) with a 10 kN load cell. Samples of $32 \times 10.5 \times 5.3$ mm were placed on a three-point bending setup with 3 mm diameter supports and a 6 mm diameter loading nose. The span was set to 20 mm and a testing speed of 1 mm/min was used. The interlaminar shear strength was calculated from the maximum applied force (F_m) via:

$$ILSS = 0.75 \frac{F_m}{w \cdot t} \tag{2}$$

where w and t represent the sample width and thicknesses, respectively. A minimum of four tests were carried out per sample type and all samples failed in shear.

Young's moduli of the produced FRP samples were evaluated by measuring the ultrasonic resonance frequency by a Grindosonic Mk5 (Lemmens NV, Belgium) device. Rectangular samples with dimensions similar to those used in DMA measurements were used. Young's modulus was calculated following ASTM standard E1876.

CRediT authorship contribution statement

Jeroen Staal: Conceptualization, Formal analysis, Investigation, Methodology, Validation, Visualization, Writing – original draft. **Baris Caglar:** Conceptualization, Formal analysis, Methodology, Supervision, Writing – review & editing. **Véronique Michaud:** Conceptualization, Funding acquisition, Project administration, Supervision, Writing – review & editing.

Declaration of competing interest

The authors declare that they have no known competing financial interests or personal relationships that could have appeared to influence the work reported in this paper.

Data availability

Data will be made available on request.

Acknowledgements

Appendix A. Supplementary data

Supplementary data to this article can be found online at https://doi.org/10.1016/j.compscitech.2024.110584.

References

[1] S. Rana, R. Fangueiro, Advanced Composite Materials for Aerospace Engineering, Woodhead Publishing, 2016, https://doi.org/10.1016/B978-0-08-100037-3.00001-8.

[2] A.A. Baker, M.L. Scott, Composite Materials for Aircraft Structures, third ed., American Institute of Aeronautics and Astronautics, Inc., 2016 https://doi.org/10.2514/4.103261.

[3] K. Friedrich, A.A. Almajid, Manufacturing aspects of advanced polymer composites for automotive applications, Appl. Compos. Mater. 20 (2013) 107–128, https://doi.org/10.1007/s10443-012-9258-7.

[4] P. Brøndsted, H. Lilholt, A. Lystrup, Composite materials for wind power turbine blades, Annu. Rev. Mater. Res. 35 (2005) 505–538, https://doi.org/10.1146/annurev.matsci.35.100303.110641.

[5] D. Abliz, Y. Duan, L. Steuernagel, L. Xie, D. Li, G. Ziegmann, Curing methods for advanced polymer composites - a review, Polym. Polym. Compos. 21 (2013) 341–348, https://doi.org/10.1177/096739111302100602.

[6] M.G. Collinson, M.P. Bower, T.J. Swait, C.P. Atkins, S.A. Hayes, B. Nuhiji, Novel composite curing methods for sustainable manufacture: a review, Compos. Part C Open Access 9 (2022), https://doi.org/10.1016/j.jcomc.2022.100293.

[7] J.A. Pojman, Cure-on-Demand composites by frontal polymerization, Encycl. Mater. Plast. Polym. (2022) 85–100, https://doi.org/10.1016/b978-0-12-820352-1.00201-7.

[8] B.A. Suslick, A.N. Yazdani, M.M. Cencer, J.E. Paul, N.A. Parikh, K.J. Stawiasz, I.P. S. Qamar, N.R. Sottos, J.S. Moore, Storable, dual-component systems for frontal ring-opening metathesis polymerization, Macromolecules (2022), https://doi.org/10.1021/acs.macromol.2c00775.

[9] J.A. Pojman, Frontal Polymerization, Elsevier B.V., 2012, https://doi.org/10.1016/B978-0-444-53349-4.00124-2.

[10] I.D. Robertson, M. Yourdkhani, P.J. Centellas, J.E. Aw, D.G. Ivanoff, E. Goli, E. M. Lloyd, L.M. Dean, N.R. Sottos, P.H. Geubelle, J.S. Moore, S.R. White, Rapid energy-efficient manufacturing of polymers and composites via frontal polymerization, Nature 557 (2018) 223–234, https://doi.org/10.1038/s41586-018-0054-x.

[11] L.M. Dean, A. Ravindra, A.X. Guo, M. Yourdkhani, N.R. Sottos, Photothermal initiation of frontal polymerization using carbon nanoparticles, ACS Appl. Polym. Mater. (2020), https://doi.org/10.1021/acsapm.0c00726.

[12] K.J. Stawiasz, J.E. Paul, K.J. Schwarz, N.R. Sottos, J.S. Moore, Photoexcitation of Grubbs' second-generation catalyst initiates frontal ring-opening metathesis polymerization, ACS Macro Lett. 9 (2020) 1563–1568, https://doi.org/10.1021/acsmacrolett.0c00486.

[13] D.G. Ivanoff, J. Sung, S.M. Butikofer, J.S. Moore, N.R. Sottos, Cross-linking agents for enhanced performance of thermosets prepared via frontal ring-opening metathesis polymerization, Macromolecules (2020), https://doi.org/10.1021/acs.macromol.0c01530.

[14] B.A. Suslick, J. Hemmer, B.R. Groce, K.J. Stawiasz, P.H. Geu, G. Malucelli, A. Mariani, J.S. Moore, J.A. Pojman, N.R. Sot, Frontal Polymerizations, From chemical perspectives to macroscopic properties and applications, Mater. Chem. (2023), https://doi.org/10.1021/acs.chemrev.2c00686.

[15] E.M. Lloyd, J.C. Cooper, P. Shieh, D.G. Ivanoff, N.A. Parikh, E.B. Mejia, K.E. L. Husted, L.C. Costa, N.R. Sottos, J.A. Johnson, J.S. Moore, Efficient manufacture, deconstruction, and upcycling of high-performance thermosets and composites, ACS Appl. Eng. Mater. 1 (2023) 477–485, https://doi.org/10.1021/acsaenm.2c00115.

[16] O. Davydovich, J.E. Paul, J.D. Feist, J.E. Aw, F.J. Balta Bonner, J.J. Lessard, S. Tawfick, Y. Xia, N.R. Sottos, J.S. Moore, Frontal polymerization of dihydrofuran comonomer facilitates thermoset deconstruction, Chem. Mater. (2022), https://doi.org/10.1021/acs.chemmater.2c02045.

[17] I.D. Robertson, L.M. Dean, G.E. Rudebusch, N.R. Sottos, S.R. White, S. Moore, Alkyl phosphite inhibitors for frontal ring-opening metathesis polymerization greatly increase pot life, ACS Macro Lett. (2017) 609–612, https://doi.org/10.1021/acsmacrolett.7b00270.

[18] D. Bomze, P. Knaack, T. Koch, H. Jin, R. Liska, Radical induced cationic frontal polymerization as a versatile tool for epoxy curing and composite production, J. Polym. Sci. Part A Polym. Chem. 54 (2016) 3751–3759, https://doi.org/10.1002/pola.28274.

[19] A. Mariani, S. Bidali, S. Fiori, M. Sangermano, G. Malucelli, R. Bongiovanni, A. Priola, UV-ignited frontal polymerization of an epoxy resin, J. Polym. Sci. Part A Polym. Chem. 42 (2004) 2066–2072, https://doi.org/10.1002/pola.20051.

[20] D. Bomze, P. Knaack, R. Liska, Successful radical induced cationic frontal polymerization of epoxy-based monomers by C-C labile compounds, Polym. Chem. 6 (2015) 8161–8167, https://doi.org/10.1039/c5py01451d.

[21] P. Knaack, N. Klikovits, A.D. Tran, D. Bomze, R. Liska, Radical induced cationic frontal polymerization in thin layers, J. Polym. Sci. Part A Polym. Chem. 57 (2019) 1155–1159, https://doi.org/10.1002/pola.29375.

[22] A. Dung Tran, T. Koch, P. Knaack, R. Liska, Radical induced cationic frontal polymerization for preparation of epoxy composites, Compos. Part A Appl. Sci. Manuf. 132 (2020) 105855, https://doi.org/10.1016/j.compositesa.2020.105855.

[23] B. Gachet, M. Lecompère, C. Croutxé-Barghorn, D. Burr, G. L'Hostis, X. Allonas, Highly reactive photothermal initiating system based on sulfonium salts for the photoinduced thermal frontal cationic polymerization of epoxides: a way to create carbon-fiber reinforced polymers, RSC Adv. 10 (2020) 41915–41920, https://doi.org/10.1039/d0ra07561b.

[24] P.J. Centellas, M. Yourdkhani, S. Vyas, B. Koohbor, P.H. Geubelle, N.R. Sottos, Rapid multiple-front polymerization of fiber-reinforced polymer composites, Compos. Part A Appl. Sci. Manuf. 158 (2022) 106931, https://doi.org/10.1016/j.compositesa.2022.106931.

[25] J. Staal, E. Smit, B. Caglar, V. Michaud, Thermal management in radical induced cationic frontal polymerisation for optimised processing of fibre reinforced polymers, Compos. Sci. Technol. 237 (2023) 110009, https://doi.org/10.1016/j.compscitech.2023.110009.

[26] N. Klikovits, P. Knaack, D. Bomze, I. Krossing, R. Liska, Novel photoacid generators for cationic photopolymerization, Polym. Chem. 8 (2017) 4414–4421, https://doi.org/10.1039/c7py00855d.

[27] R. Taschner, P. Knaack, R. Liska, Bismuthonium- and pyrylium-based radical induced cationic frontal polymerization of epoxides, J. Polym. Sci. (2021) 1–14, https://doi.org/10.1002/pol.20210196.

[28] R. Taschner, R. Liska, P. Knaack, Evaluation of suitable onium tetrafluoroborates for cationic polymerization of epoxides, Polym. Int. (2021), https://doi.org/10.1002/pi.6330.

[29] R. Taschner, R. Liska, P. Knaack, Iodonium borate initiators for cationic photopolymerization and their application in radical-induced cationic frontal polymerization, ACS Appl. Polym. Mater. (2022), https://doi.org/10.1021/acsapm.2c01465.

[30] B.R. Groce, D.P. Gary, J.K. Cantrell, J.A. Pojman, Front velocity dependence on vinyl ether and initiator concentration in radical-induced cationic frontal polymerization of epoxies, J. Polym. Sci. (2021) 1–8, https://doi.org/10.1002/pol.20210183.

[31] I. Naseri, M. Yourdkhani, Rapid and energy-efficient frontal curing of multifunctional composites using integrated nanostructured heaters, ACS Appl. Mater. Interfaces 14 (2022) 50215–50224, https://doi.org/10.1021/acsami.2c15415.

[32] M.S. Malik, M. Wolfahrt, S. Schlögl, Redox cationic frontal polymerization: a new strategy towards fast and efficient curing of defect-free fiber reinforced polymer composites, RSC Adv. 13 (2023) 28993–29003, https://doi.org/10.1039/d3ra05976f.

[33] D. Salvatori, B. Caglar, H. Teixidó, V. Michaud, Permeability and capillary effects in a channel-wise non-crimp fabric, Compos. Part A. 108 (2018) 41–52, https://doi.org/10.1016/j.compositesa.2018.02.015.

[34] D. Salvatori, B. Caglar, V. Michaud, 3D spacers enhance flow kinetics in resin transfer molding with woven fabrics, Compos. Part A Appl. Sci. Manuf. 119 (2019) 206–216, https://doi.org/10.1016/j.compositesa.2019.01.023.

[35] W.D. Brouwer, E.C.F.C. Van Herpt, M. Labordus, Vacuum injection moulding for large structural applications, Compos. Part A Appl. Sci. Manuf. 34 (2003) 551–558, https://doi.org/10.1016/S1359-835X(03)00060-5.

[36] J.F.A. Kessels, A.S. Jonker, R. Akkerman, Optimising the flow pipe arrangement for resin infusion under flexible tooling, Compos. Part A Appl. Sci. Manuf. 38 (2007) 2076–2085, https://doi.org/10.1016/j.compositesa.2007.04.008.

[37] J. Wang, P. Simacek, S.G. Advani, Use of medial axis to find optimal channel designs to reduce mold filling time in resin transfer molding, Compos. Part A Appl. Sci. Manuf. 95 (2017) 161–172, https://doi.org/10.1016/j.compositesa.2017.01.003.

[38] N. Montés, F. Sánchez, A new computational tool for liquid composite moulding process design based on configuration spaces, Compos. Part A Appl. Sci. Manuf. 41 (2010) 58–77, https://doi.org/10.1016/j.compositesa.2009.07.003.

[39] E. Goli, N.A. Parikh, M. Yourdkhani, N.G. Hibbard, J.S. Moore, N.R. Sottos, P. H. Geubelle, Frontal polymerization of unidirectional carbon-fiber-reinforced composites, Compos. Part A Appl. Sci. Manuf. 130 (2020) 105689, https://doi.org/10.1016/j.compositesa.2019.105689.

[40] E. Goli, I.D. Robertson, H. Agarwal, E.L. Pruitt, J.M. Grolman, P.H. Geubelle, J. S. Moore, Frontal polymerization accelerated by continuous conductive elements, J. Appl. Polym. Sci. 47418 (2018) 1–9, https://doi.org/10.1002/app.47418.

[41] Y. Gao, F. Shaon, A. Kumar, S. Bynum, D. Gary, D. Sharp, J.A. Pojman, P. H. Geubelle, Rapid frontal polymerization achieved with thermally conductive metal strips, Chaos 31 (2021) 21–24, https://doi.org/10.1063/5.0052821.

[42] M.S. Malik, V. Grasser, M. Wolfahrt, S. Schlögl, Addressing the challenges in frontal curing of high- performance carbon fiber reinforced composites, in: 20th Eur. Conf. Compos. Mater., 2022, pp. 1–7.